Energy 266 (2023) 126459

Contents lists available at ScienceDirect

Energy

journal homepage: www.elsevier.com/locate/energy

Waste heat recovery solution based on a heat pipe heat exchanger for the aluminium die casting industry

Hussam Jouhara [a,e,*], Nerea Nieto [b], Bakartxo Egilegor [b], Josu Zuazua [c], Eva González [c], Ignacio Yebra [d], Alfredo Igesias [d], Bertrand Delpech [a], Sulaiman Almahmoud [a], Daniel Brough [a], Jurgita Malinauskaite [a], Antonis Vlasopoulos [a], Mark Hill [a], Brian Axcell [a]

[a] Heat Pipe and Thermal Management Research Group, Brunel University London, Uxbridge, UB8 3PH, UK
[b] Ikerlan, Technology Research Centre, 20500, Arrasate-Mondragón, Spain
[c] Fagor Ederlan S.Coop, 20500, Arrasate-Mondragón, Spain
[d] Insertec, 48970, Basauri, Spain
[e] Vytautas Magnus University, Studentu Str. 11, LT-53362, Akademija, Kaunas Distr., Lithuania

ARTICLE INFO

Keywords:
Heat Pipes
Waste heat recovery
Energy efficiency
Aluminium die casting industry

ABSTRACT

An analysis of the end use of energy in the EU reveals that industry is one of the three dominant categories, which accounts for 26.1% of the final end use of energy. In the case of the aluminium industry, approximately 70% of energy consumption is due to heat and thermal processes, highlighting a vast potential for waste heat recovery technologies. Within the aluminium die casting industry, liquid aluminium is cast, formed, cooled, and further processed within a thermal heat process, which includes three sub-processes: solubilising, quenching, and ageing. In the case presented, a thermal heat process is the second most energy intensive process within the factory, and the ageing heat treatment furnace accounts for 15% of the thermal heat process. The thermal heat treatment generates a significant amount of waste heat. The recovery of that waste heat, with minimal risk of cross contamination between streams and reduced chance of equipment failure, has been achieved via the use of a heat pipe heat exchanger (HPHE). The HPHE has been designed, manufactured, and installed in the solution furnace exhaust stack. The HPHE was designed to recover up to 88.6 kW in steady state operating conditions at 400 °C. The return on investment has been evaluated at 35 months with an expected CO_2 emissions reduction of 86 tCO_2/year when best engineering practices are applied. Furthermore, a theoretical modelling tool to predict the thermal performance of the HPHE was developed and validated within a ±20% deviation from the experimental results. This paper further presents the development of the theoretical model to allow a characterisation of HPHE technology and will act as a guideline for the design of HPHEs within the aluminium industry.

1. Introduction

The ETEKINA project (heat pipE TECHnologies for INdustrial Applications) began in 2017 with the goal of employing heat pipe heat exchangers (HPHE) in a number of energy intensive industries for waste heat recovery and targeted recovering 57–70% of the waste heat stream in those industries [1,2]. The need for such increases in efficiency is pressing and will allow for both financial and environmental savings in the industrial and manufacturing sectors, which contribute 26.2% and 15.6% to global GDP [3], respectively. With global emissions returning to pre-COVID-19 levels of 33.0 $GtCO_2e$ in 2021 [4], the EU target reduction of 83–87% CO_2 reduction by 2050 [5,6] cannot be met completely by waste heat recovery, however it is obvious that the relative quality of that waste heat in many industries will yield suitable areas of development and exploitation [7,8]. Miro, Brueckner et al. [9] studied the cumulative waste heat outputs of 33 countries and highlighted the relative potential for energy recovery across 6 main industries, as shown in Fig. 1. The ETEKINA project addresses a number of these sectors, but the non-ferrous metal sector is of interest to this paper, whose share of energy can account for approximately 22% of the production costs [10,11].

Brueckner, Miro et al. [12] reviewed a variety of methods used in estimating waste heat production and highlighted the general availability of excess high-grade heat, as shown in Fig. 2, where metal production and processing is one of the major sources of excess, high grade

* Corresponding author. Heat Pipe and Thermal Management Research Group, Brunel University London, Uxbridge, UB8 3PH, UK.
E-mail address: hussam.jouhara@brunel.ac.uk (H. Jouhara).

https://doi.org/10.1016/j.energy.2022.126459
Received 18 October 2022; Received in revised form 1 December 2022; Accepted 16 December 2022
Available online 17 December 2022

Nomenclature

Symbols Unit

A	Surface area m^2
A_{1e}	Bare area for the heat pipe in the evaporator m^2
A_{1c}	Bare area for the heat pipe in the condenser m^2
A_{2e}	Fin area for the heat pipe in the evaporator m^2
A_{2c}	Fin area for the heat pipe in the condenser m^2
C	Heat capacity rate $W.K^{-1}$
Cst	Cost £.$year^{-1}$
C_P	Specific heat capacity $J.kg^{-1}.K^{-1}$
C_r	Heat capacity ratio, ($C_r = C_{min}/C_{max}$) dimensionless
C_{sf}	Constant in *Rohsenow* correlation depending on the surface-fluid combination dimensionless
D	Diameter m
E	Energy kWh
g	Gravitational acceleration $m.s^{-2}$
h	Heat transfer coefficient $W.m^{-2}.K^{-1}$
h_{fg}	Latent heat of vaporisation $J.kg^{-1}$
k	Thermal conductivity of the heat pipe wall $W.m^{-2}.K^{-1}$
K_e	Equivalent heat transfer coefficient accounts for the contribution of the pipe walls and evaporation $W.m^{-2}.K^{-1}$
K_c	Equivalent heat transfer coefficient that accounts for the contribution of pipe walls and condensation $W.m^{-2}.K^{-1}$
L	Length m
$\dot{m}$	Mass flow rate $kg.s^{-1}$
n_{total}	Number of pipes
Nu	Nusselt number, ($Nu = hD/k$) dimensionless
P_{fin}	Fin pitch m
Pr	Prandtl number, ($Pr = \mu c_p/k$) dimensionless
Q	Heat transfer rate W
R	Thermal resistance $°C.W^{-1}$
R_{time}	Working hours hr
Re	Reynolds number, ($Re = \rho VD/\mu$) dimensionless
S_L	Longitudinal pitch of the staggered arrangement m
S_T	Transverse pitch of the staggered arrangement m
T	Temperature K
U	Overall heat transfer coefficient $W.m^{-2}.K^{-1}$
V	Velocity $m.s^{-1}$

Greek Symbols

Δ	Difference
ε	Effectiveness dimensionless
η	Efficiency dimensionless
ρ	Density $kg.m-3$
σ	Surface tension $N.m^{-1}$
μ	Dynamic viscosity Pa.s
χ^*	Ratio of pipe pitch to pipe diameter dimensionless

Subscripts

c	Refers to condenser section
ci	Internal surface of the condenser
co	External surface of the condenser
$cond$	Conduction
e	Refers to evaporator section
ei	Internal surface of the evaporator
eo	External surface of the evaporator

exp Experimental

f	Fin
h	Heat
hp	Heat Pipe
$HPHE$	Heat Pipe Heat Exchanger
l	Liquid
L	Longitudinal
LM	Logarithmic
max	Maximum
NG	Natural gas
o	Outer
out	Outlet
s	Wall surface
sat	Saturation
T	Transverse
theo	Theoretical
v	Vapour

Acronym

$\dot{m}_{PSt}$	Mass flow rate Primary Stream (Evaporator of the HPHE)
$\dot{m}_{SStm}$	Mass flow rate Secondary Stream (Condenser of the HPHE)
T_{PSt_in}	Temperature Primary Stream (exhaust), inlet of the HPHE
T_{PSt_Out}	Temperature Primary Stream (exhaust), outlet of the HPHE
T_{SSt_In}	Temperature Secondary Stream (air), inlet of the HPHE
T_{SSt_Out}	Temperature Secondary Stream (air), outlet of the HPHE

heat (≥350 °C).

The significance of high grade heat in waste heat recovery is an important consideration in maximising industrial plant efficiency [13]. Recovery temperatures between 230 and 650 °C generally minimise the effects of thermal stress on heat exchange materials and surfaces, reduce emissions (CO_2, SOx, NOx and UHCs) but avoid the possibility of corrosive substances condensing in heat exchangers during the heat recovery process [14–16]. Waste heat recovery is not limited to reuse within a process and can also be considered for use in other processes or as a direct heat source to generate steam for power or heating efficiency increases [16–18], thus there are a number of areas in aluminium production that can be considered for the use of waste heat recovery.

Of particular interest in the non-ferrous sector is that of aluminium die casting. This activity is energy intensive and requires a heat input in almost all parts of the typical process. The intensive use of energy in the sector makes the competitiveness of European companies more challenging, since energy costs in Europe are typically more expensive than in other parts of the world where aluminium die casting is undertaken [10,11,19,20] Therefore, heat recovery is an important consideration. Whilst direct comparison with most countries in the use of both electricity and natural gas is possible, it should be noted that the non-ferrous metal production industry in China relies more on coal as a primary fuel than natural gas and thus very few comparisons are possible from a cost perspective. Yanjia and Chandler [21] reported that oil and natural gas usage in China represented only 5% of the total energy consumption, with coal (52%) and electricity (43%) being the dominant energy sources. This is typical of aluminium production, although natural gas usage in production can be seen to have increased in the period 2010–2020 [22,23].

In parallel industries, Ros-Dosdá et al. [24] assessed 25 existing energy reduction techniques in ceramics production and assessed, through Life Cycle Analysis (LCA), that the EU 2050 target can only be met if both endogenous and exogenous technologies are applied to the manufacturing process; of the endogenous techniques energy efficiency of the thermal processes alone would see the greatest CO_2 reduction. This general trend is also seen in industries centred around aluminium die casting where heat recovery is considered a priority for efficiency increases with additional enhancements in process improvement such as recycling of material and water reuse being further considered [21, 25–27]. Bonila-Campos et al. [26], in particular, highlight that energy

efficiency and process improvements are crucial to realise financial and environmental savings in the aluminium die casting industry.

The non-ferrous metal sector shows an economic and technical potential for the reduction of energy consumption [14,28,29]. The EU report [28] predicts a possible 22% reduction in energy usage or 21% by 2050. The reductions in these predictions are largely due to a projected stagnation in the production of aluminium. One aspect of this analysis which gives credence to the consideration of process waste heat recovery is that the reduction is predicated on the increased use of secondary (recycled) aluminium which is recognised as being critical to efficiency increases in aluminium production [22]. This ignores the technical benefits of energy reduction associated with heat recovery and the re-use of waste heat which is the focus of the ETEKINA project and which could lead to substantial additional financial and environmental savings. The waste heat recovery potential as an energy efficiency measure applied to the aluminium industry was studied by Brough et al. [17], who highlighted the potential use of the HPHE in the aluminium industry, whilst an in-depth study by Egilegor, Jouhara et al. [30] placed the HPHE under the ETEKINA framework as a method of waste heat recovery for steel and ceramics manufacturing as well. Simulation models of processes studied in the ETEKINA project centred around the recovery of heat from a solution heat treatment furnace to be used in an ageing heat treatment furnace with an expected energy consumption reduction of between 50% and 80% in the burners of the ageing furnace, dependent on burner position, based on the analysis of Bonila-Campos et al. [26].

In this paper the performance of a HPHE waste heat recovery system, with a nominal capacity of 89 kW, installed in the thermal treatment furnaces of aluminium automotive parts is described. Subsequent sections describe a general oveview of HPHE technology, the waste heat recovery solution as designed for a low pressure aluminium die casting facility, and how the solution was implemented. In the final sections, the main results of the waste heat recovery solution from both an energetic and economic point of view are highlighted and, finally, the main conclusions derived from the implementation are summarised.

2. General overview of the HPHE technology

HPHEs are constructed from a number of independent vertically mounted "heat pipes" which can be configured to best suit the geometry of the application that they are to be used in. Typically the heat pipes are

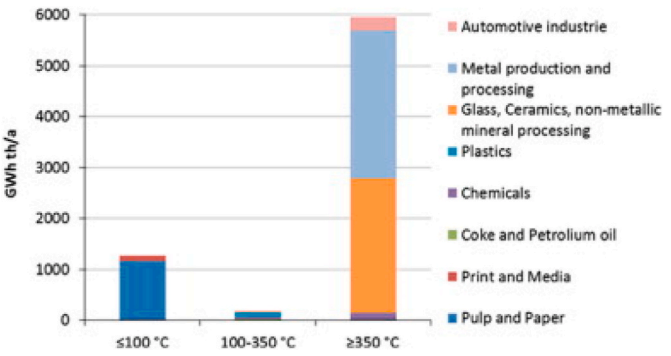

Fig. 2. *Cumulative waste heat quantity showing the availability of heat in various industries and applications* [12].

used in either a staggered or inline array and can be internally configured to contain a number of passes or baffled, as would be expected of a traditional heat exchanger. Increasing the number of passes typically improves performance in full-scale heat exchangers with minimal effect on maintenance [31–34]. A heat pipe and HPHE are shown in Fig. 3.

In the heat pipe, the lower portion is exposed to the "hot" stream and the upper to the "cold" stream of the process flows. Each pipe is hermetically sealed and contains a fluid, which can be chosen to have suitable evaporating and condensing temperatures to complement the process operating parameters. In operation, the heat pipe allows the working fluid to transport heat between condenser and evaporator sections internally without the use of an internal wick, as opposed to conventional, smaller diameter, heat pipes, which are limited in size and capacity by capillary pumping pressure [35]. A variety of contributing factors such as fluid fill ratios, heat pipe inclination and, in particular, the modelling of geyser boiling within HPHEs has been studied by Jouhara et al. [36], allowing the processes within the heat pipe itself to be understood to exact optimum operational conditions, minimising the effects of heat pipe dry out and keeping heat transfer rates high [37–41].

3. Methodology

3.1. Application concept

The objective of the HPHE system implementation developed under

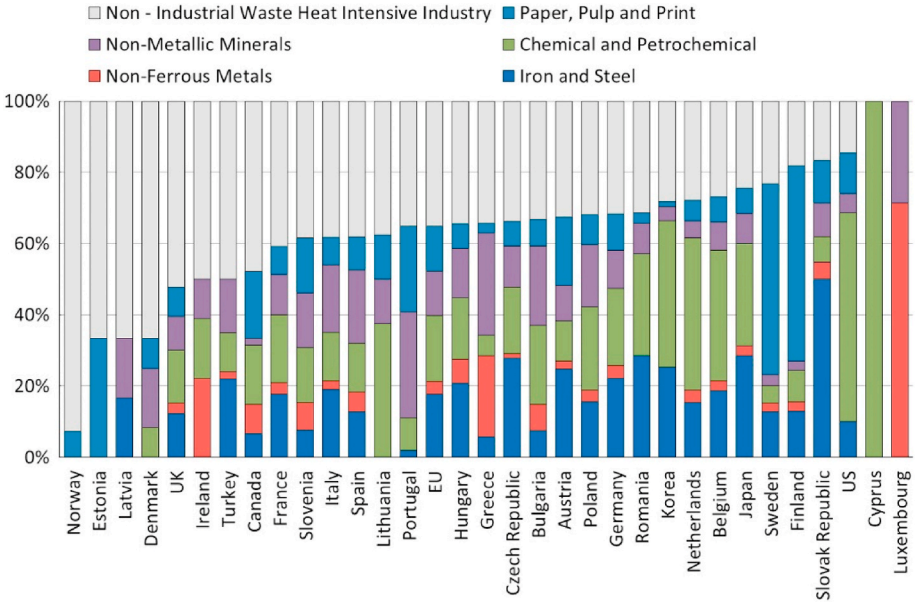

Fig. 1. *Industrial Waste Heat Intensive Industries* [9].

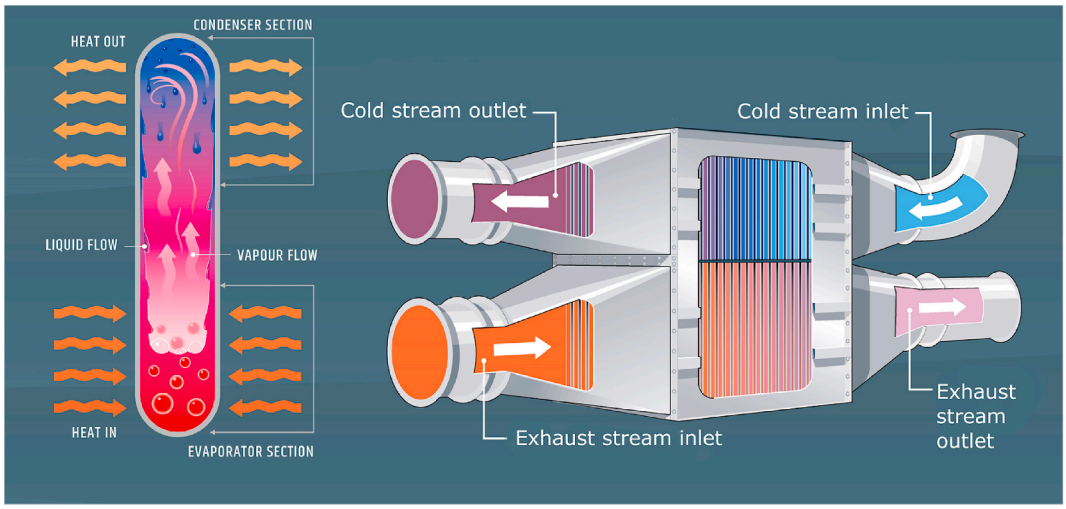

Fig. 3. Heat Pipe and HPHE concept.

the ETEKINA project framework and described in this paper is to improve the energy performance of the non-ferrous metal industrial sector, represented in this case by a low pressure die casting facility of Fagor Ederlan S. Coop. The aim is to demonstrate the economic feasibility and the market potential of HPHE implementation in the non-ferrous metal sectors.

The aluminium knuckles manufactured by the facility are shown in Fig. 4 and require specific metallurgic properties to comply safely with their function of connecting crucial automobile components such as suspension arms, tie rods and wheel bushings. The aluminium knuckles acquire their specific metallurgical characteristics by being subjected to progressive heat treatments.

Three heat treatment processes are undertaken as shown in Fig. 5. The initial treatment consists of heating components to 540 °C in a Solution Heat Treatment Furnace (SHTF), following which they are immersed in a Quenching Tank (QT) and rapidly cooled to 40 °C, finally the parts are reheated to 160 °C in an Ageing Heat Treatment Furnace (AHTF). Both furnaces (solution and ageing) are a roller-hearth continuous type with natural gas fired heating. Components cross the furnaces in baskets that are moved by rollers. The goal of the HPHE system is to capture the waste thermal energy of the solution furnace exhaust fumes and use it in the ageing furnace. Fig. 6 shows the layout of the HPHE system.

The HPHE specifications were based on measured flow rates and temperatures of the exhaust gases of the solution furnace and measurements of the ageing furnace gas consumption. The HPHE was designed to operate at high secondary stream temperatures, with no cross contamination, a high heat transfer to plant footprint ratio and high controllability of its performance. The HPHE unit was designed to recover 89 kW based on 1791 kg h^{-1} of exhaust fumes at 400 °C and a secondary stream flow rate of 1802 kg h^{-1} at 145 °C.

Fig. 4. Automotive aluminium parts manufactured by Fagor Ederlan S. Coop.

3.2. HPHE design

The designed HPHE was manufactured and integrated in the low pressure die casting plant of Fagor Ederlan. S. Coop. The HPHE design for this application is an air to air crossflow HPHE. The evaporator section, located at the lower section allows the recovery of heat from the exhaust flow. The inlet for the upper section is air from the ageing furnace, recirculated at the inlet of the ageing furnace. The heat recovered from the evaporator is subsequently transferred to the heat sink fluid via the condenser section. An illustration of the HPHE can be seen in Figs. 7 and 8.

The HPHE comprises 310 heat pipes installed in a staggered arrangement. Two working fluids are employed in the heat exchanger bundles: distilled water and Dowtherm™ as shown in Fig. 9. Splitting the HPHE into two sections allows for a much higher temperature output as the maximum working temperature of the Dowtherm™ heat pipe bundle is higher than that of the water heat pipe bundle.

3.3. Theoretical modelling

The HPHE transfers heat from the hot exhaust stream to the cold air stream through the heat pipes. Each heat pipe transfers heat independently, acting as an individual heat exchanger. Heat is transferred from the exhaust stream to the outside of the heat pipe wall predominantly by forced convection. The heat then transfers to the inner side of the wall by thermal conduction. As a result, the saturated liquid in the heat pipe evaporator boils and the vapour flows to the condenser, due to a small pressure difference between the evaporator and the condenser. The saturated vapour condenses at the condenser, releasing heat to the inner side of the condenser wall. The heat then transfers to the outside of the wall by thermal conduction. Finally, heat transfers from the outer condenser wall to the air by forced convection. The heat transfer process can be modelled as a series of thermal resistances, analogous to electrical resistances, as illustrated in Fig. 10, where the main driving force is the temperature difference between the exhaust gas stream and the air stream.

The total thermal resistance of a single heat pipe, R_{hp}, can be obtained by Ref. [42]:

$$R_{hp} = R_{eo} + R_{cond\_e} + R_{ei} + R_{ci} + R_{cond\_c} + R_{co} \quad (1)$$

where R_{eo} and R_{co} correspond to the forced convection heat transfer resistances at the evaporator and condenser. R_{cond_e} and R_{cond_c} are the wall radial conduction at the evaporator and condenser. R_{ei} and R_{co} represent the boiling and condensation resistances of the heat pipe

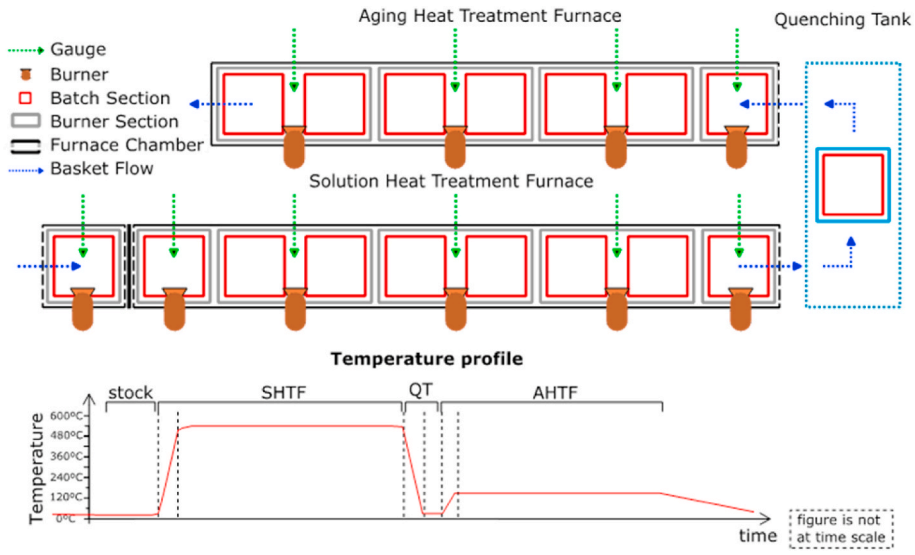

Fig. 5. Scheme of heat treatment process.

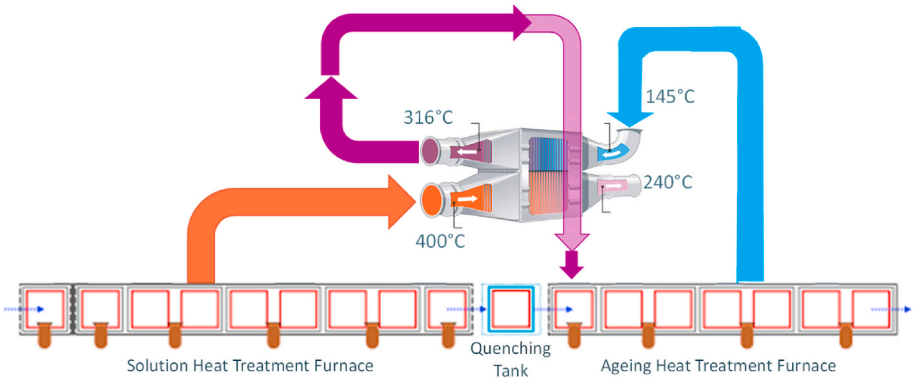

Fig. 6. Layout of the WHR system based on a HPHE applied in thermal treatment furnaces of aluminium automotive parts.

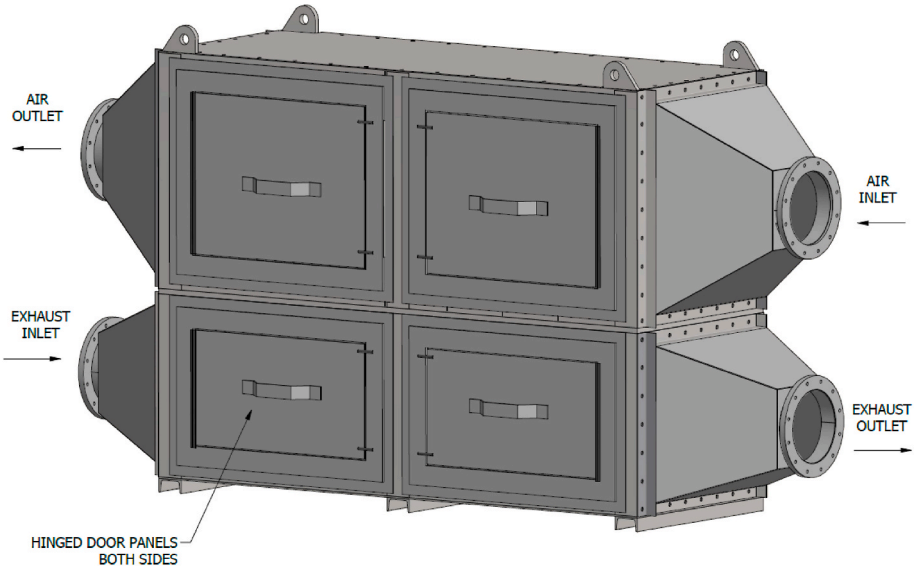

Fig. 7. HPHE 3D view.

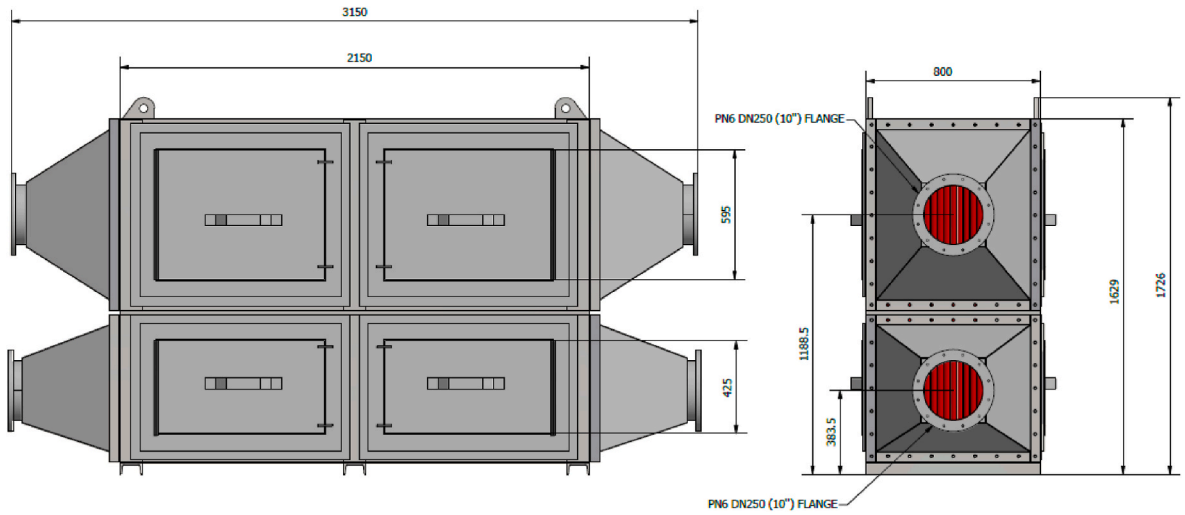

Fig. 8. HPHE General arrangement and dimensions.

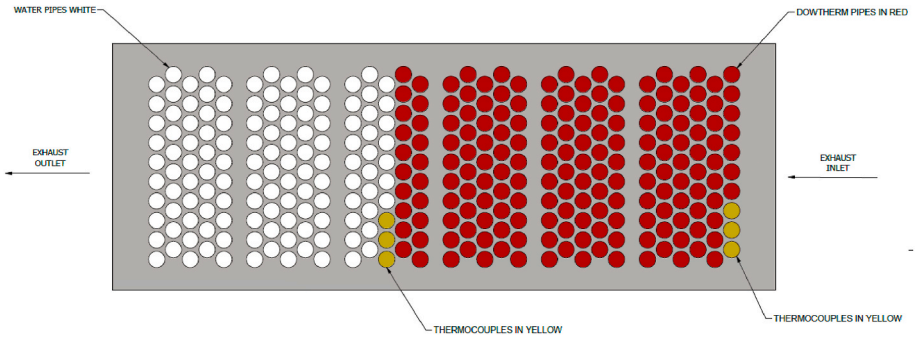

Fig. 9. Diagram of separation plate showing heat pipe arrangement.

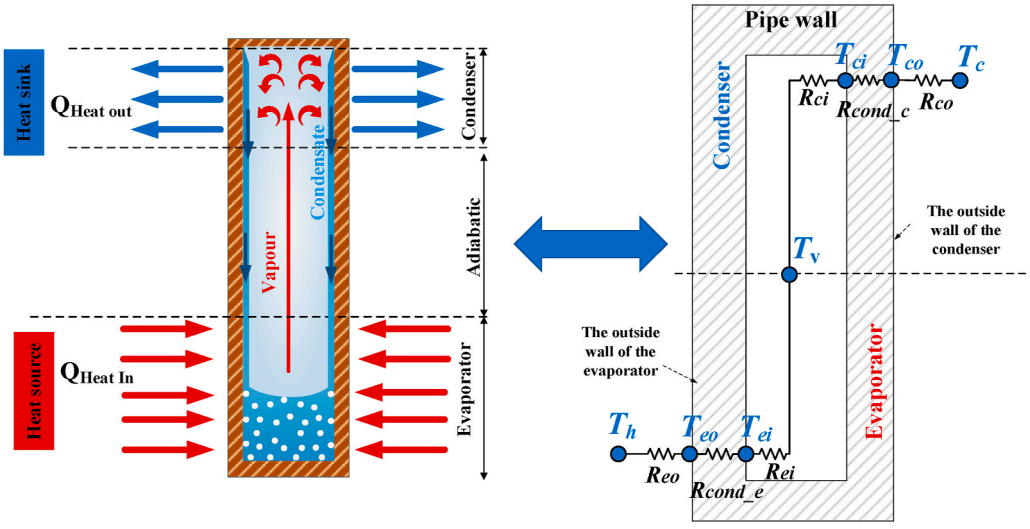

Fig. 10. Two-phase working cycle of a heat pipe and its corresponding thermal resistance model.

($K{\cdot}W^{-1}$), respectively. The boiling and condensation resistances are obtained from the relation between thermal resistance and the heat transfer coefficient, as follows:

$$R = \frac{1}{hA} \tag{2}$$

with R being the thermal resistance (K. W^{-1}), h the heat transfer coefficient ($W.m^{-2}$. K^{-1}), and A the heat transfer surface area (m^2).

The heat transfer coefficient for boiling is obtained from the correlation provided by *Rohsenow* [43], which is recommended for a wide range of applications [44]:

$$h_{boiling} = \mu_l . h_{fg} \left[\frac{g.(\rho_l - \rho_v)}{\sigma}\right]^{\frac{1}{2}} \left[\frac{C_P}{(C_{sf}.h_{fg}.Pr_l^n)}\right]^3 .(T_{ei} - T_v)^2 \quad (3)$$

where μ_l is the liquid dynamic viscosity (Pa.s), h_{fg} is the latent heat of vaporisation (J.kg^{-1}), g is the gravitational acceleration (m.s^{-2}), ρ_l and ρ_v are the liquid and vapour densities (kg.m^{-3}), σ is the working fluid surface tension (N.m^{-1}), $Pr_l = \mu_l C_{P,l}/k_l$ is the liquid Prandtl number, C_P is the specific heat capacity (J.kg^{-1}. K^{-1}), k_l is the thermal conductivity of the liquid (W.m^{-1}. K^{-1}), C_{sf} is a constant depending on the surface-fluid combination which is 0.0132 for this heat pipe material-working fluid combination design, and T_{ei} and T_v are the evaporator inner wall side and the saturation temperatures (K), respectively.

The heat transfer coefficient for condensation is calculated using the Nusselt [45] correlation [46]:

$$h_{condensation} = 0.943 \left[\frac{\rho_l(\rho_l - \rho_v)h_{fg}gk_l^3}{\mu_l L_c(T_{sat} - T_{ci})}\right]^{1/4} \quad (4)$$

where ρ_l and ρ_v are the liquid and vapour densities (kg.m-3), h_{fg} is the latent heat of vaporisation (J.kg-1), g is the gravitational acceleration (m.s-2), k_l is the thermal conductivity of the liquid (W.m-1. K-1), μ_l is the liquid dynamic viscosity (Pa.s), L_c is the condenser length (m), and T_{ci} is the temperature of the condenser wall (K). The radial conduction resistances of the walls at the evaporator and condenser are given as follows:

$$R_{cond} = \ln(D_o / D_i) / (2\pi L_e k_e) \quad (5)$$

$$R_{c,cond} = \ln(D_o / D_i) / (2\pi L_c k_c) \quad (6)$$

D_o and D_i represent the external and internal diameters of the heat pipe (m), respectively. k_e and k_c are the wall thermal conductivity (W.m-1. K-1) at the evaporator and condenser, respectively., and L_e and L_c are the evaporator and condenser lengths, respectively (m).

The forced convection resistance at the evaporator $R_{e,out}$ and condenser $R_{c,out}$ can be obtained by calculating the corresponding forced convection heat transfer coefficients and corresponding heat transfer area, then using Eq. (2). To determine the forced convection heat transfer coefficient of each pipe, the correlations by Zukauskas [47–49] can be used:

$$Nu = \frac{h_{F.convection} D_o}{k} = 0.192 \left(\frac{\chi_t^*}{\chi_l^*}\right)^{0.2} \left(\frac{P_{fin}}{D_o}\right)^{0.18} \left(\frac{H_f}{D_o}\right)^{-0.14} Re^{0.65} Pr^{0.36} \left(\frac{Pr}{Pr_s}\right)^{0.25} \quad (7)$$

where Nu is the Nusselt number, $h_{F.convection}$ is the forced convection heat transfer coefficient (W.m-2. K-1), k is the thermal conductivity of the fluid (W.m-1. K-1), χ_t^* is a ratio of transverse pitch to pipe diameter, χ_l^* is a ratio of longitudinal pitch to tube diameter, P_{fin} is the fin pitch, H_f is the fin height. Re is the Reynolds number, Pr and Pr_s are the Prandtl number of the flow and the Prandtl number at the surface temperature, respectively.

χ_t^* and χ_l^* are given by:

$$\chi_t^* = \frac{S_T}{D_o} \quad (8)$$

$$\chi_l^* = \frac{S_L}{D_o} \quad (9)$$

S_T and S_L are the transverse pitch and longitudinal pitch of the staggered heat exchanger (m).

The overall heat transfer area of the heat pipe for forced convection is calculated as follows:

$$A_{eo} = A_{eo,bare} + \eta_{eo} A_{eo,fins} \quad (10)$$

$$A_{co} = A_{co,bare} + \eta_{co} A_{co,fins} \quad (11)$$

where $A_{eo,bare}$ and $A_{co,bare}$ are the evaporator and condenser outer bare areas, respectively. $A_{eo,fins}$ and $A_{co,fins}$ are the fin surface areas and η_{eo} and η_{co} are the fin efficiencies at the evaporator and condenser, respectively.

The fin efficiency can be calculated from Ref. [50]:

$$\eta = \frac{\tanh(m_{fin}.Y_{fin})}{m_{fin}.Y_{fin}} \quad (12)$$

where

$$m_{fin} = \sqrt{\frac{2h_{F.convection}}{k_{fin}t_{fin}}} \quad (13)$$

$$Y_{fin} = \left(H_{fin} + \frac{t_{fin}}{2}\right)\left[1 + 0.35 \ln\left(\frac{D_{fin}}{D_o}\right)\right] \quad (14)$$

where k_{fin} is the thermal conductivity (W.m^{-1}. K^{-1}) of the fins and t_{fin} (m) is the fin thickness. Therefore, the HPHE can be modelled based on the electrical analogy approach as presented in Fig. 11.

The heat recovery of the HPHE can be determined from the following equation [51]:

$$Q = \frac{\Delta T_{LM}}{R_{HPHE}} \quad (15)$$

where R_{HPHE} total is the overall thermal resistance of the HPHE. ΔT_{LM} is the logarithmic mean temperature of the inlet and outlet of the flue gas and air streams, which can be calculated for a counter flow heat exchanger from Ref. [52]:

$$\Delta T_{LM} = \left(\frac{(T_{flue\ gas,in} - T_{air,out}) - (T_{flue\ gas,out} - T_{air,in})}{\ln\left(\frac{T_{flue\ gas,in} - T_{air,out}}{T_{flue\ gas,out} - T_{air,in}}\right)}\right) \quad (16)$$

Eq. (*15*) can be written in a different form as follows:

$$Q = UA\Delta T_{LM} \quad (17)$$

where UA is the HPHE overall conductance (W·K^{-1}).

Based on the electrical analogy in Fig. 11, the total thermal resistance R_{HPHE} of the HPHE can be obtained from the following equation [53]:

$$\frac{1}{R_{HPHE}} = \frac{1}{R_{hp,1}} + \frac{1}{R_{hp,2}} + \ldots + \frac{1}{R_{hp,n-1}} + \frac{1}{R_{hp,n}} \quad (18)$$

where R is the thermal resistance (K·W^{-1}), the subscripts hp refers to heat pipe, and n is the number of heat pipes within the heat exchanger. Assuming that the heat pipe resistance is equal for all the heat pipes, the overall thermal resistance R_{HPHE} of the heat pipe heat exchanger can be expressed as:

$$R_{HPHE} = \frac{R_{hp}}{n_{total}} \quad (19)$$

with R_{hp} the average thermal resistance of a heat pipe (K·W^{-1}), and n the number of heat pipes in the heat exchanger.

The heat transfer rate can be calculated from:

$$Q = \dot{m}_{air} C_{P,air}(T_{air,in} - T_{air,out}) \quad (20)$$

A heat exchanger is evaluated by its effectiveness which is the ratio of the actual heat transfer rate to the maximum theoretically possible heat transfer rate.

The effectiveness (ε) of the HPHE is given by the following expression [54]:

$$\varepsilon_{HPHE} = \frac{Q_{air}}{Q_{max}} \quad (21)$$

Q_{air} is the actual heat transfer rate recovered (W), and Q_{max} is the

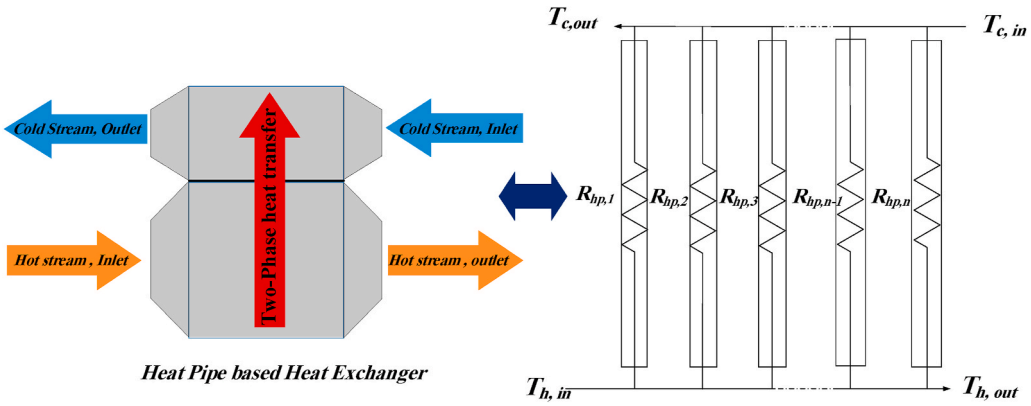

Fig. 11. Thermal electrical analogy of a HPHE.

maximum possible heat transfer rate (W). The maximum heat transfer rate achievable by a heat exchanger is dependent on the inlet temperatures of both fluids and of the minimum heat capacity rate of the fluids as follows:

$$Q_{max} = C_{min}\left(T_{flue\ gas,in} - T_{air,in}\right) \tag{22}$$

In this expression, C_{min} is the minimum heat capacity rate ($W{\cdot}K^{-1}$), and $T_{flue\ gas,in}$ and $T_{air,in}$ are the inlet temperatures of the flue gas and air streams, respectively. Eq. (22) shows that the maximum heat transfer achievable is the case where the fluid with minimum heat capacity reaches the temperature of the other fluid. Indeed, the heat capacity rate indicates the capacity of a fluid to increase its temperature for a given heat transfer rate. In this study, the fluid with minimum heat capacity rate was the air. Thus, the minimum capacity rate C_{min} can be written as:

$$C_{min} = \dot{m}_{air} C_{P,air} \tag{23}$$

where $\dot{m}_{air}$ is the air mass flow rate ($kg.s^{-1}$), and $C_{P,air}$ is the specific heat capacity of air ($J.kg^{-1}.\ K^{-1}$).

3.4. Implementation of the waste heat recovery solution in Fagor Ederlan S.Coop

The designed HPHE is located on a platform between the two furnaces investigated. The location of the HPHE can be seen in Fig. 12.

The HPHE is connected into the system according to the diagram in Fig. 13. Exhaust gases are extracted from the solution furnace stack through a bypass system, installed to isolate the HPHE in case of maintenance. The exhaust is then subjected to an air dilution valve in order to control the temperature entering the evaporator of the HPHE. The exhaust is then returned to the ageing furnace stack. On the condenser side, air is extracted from the last section of the ageing furnace. The air is then injected into the condenser section of the HPHE, the hot air is then reinjected on the first section of the ageing furnace where most of the heat is required.

Preheating loops were also installed to heat the air in the condenser section prior to injection into the solution furnace for a HPHE start at cold (i.e. after a maintenance cycle). Safety systems such as temperature control and bypass are also included.

As shown in Fig. 13, thermocouples were placed at various locations of the HPHE system. K type thermocouples were placed at the inlet (T_{PSt_In}) and outlet (T_{PSt_Out}) of the evaporator section to measure the amount of heat extracted from the exhaust. A similar setup was also used on the condenser section to measure the amount of heat transferred to the heat sink (T_{SSt_In} and T_{SSt_Out}). Three thermocouples were placed on the first row of the Dowtherm™ section and on the water section using thermowells to ensure that the temperature of the heat pipes in each section does not reach the critical working temperature, respectively. Other temperature sensors were placed at various locations of the system such as in the bypass system, in the recirculation system and at the outlet of the solution furnace.

Pitot probe sensors were also placed in each stream to measure the gas flow rates in the exhaust ($\dot{m}_{PSt}$) and heat sink ($\dot{m}_{SStm}$) sections. Finally, pressure sensors were also placed at the outlet of the solution furnace to ensure that the HPHE does not have any impact on the operating pressure of the furnace. Indicative locations of these sensors

Fig. 12. Photo of the WHR system based on HPHE installed in Fagor Ederlan S. Coop.: a) solution heat treatment furnace; b) HPHE; c) ageing heat treatment furnace.

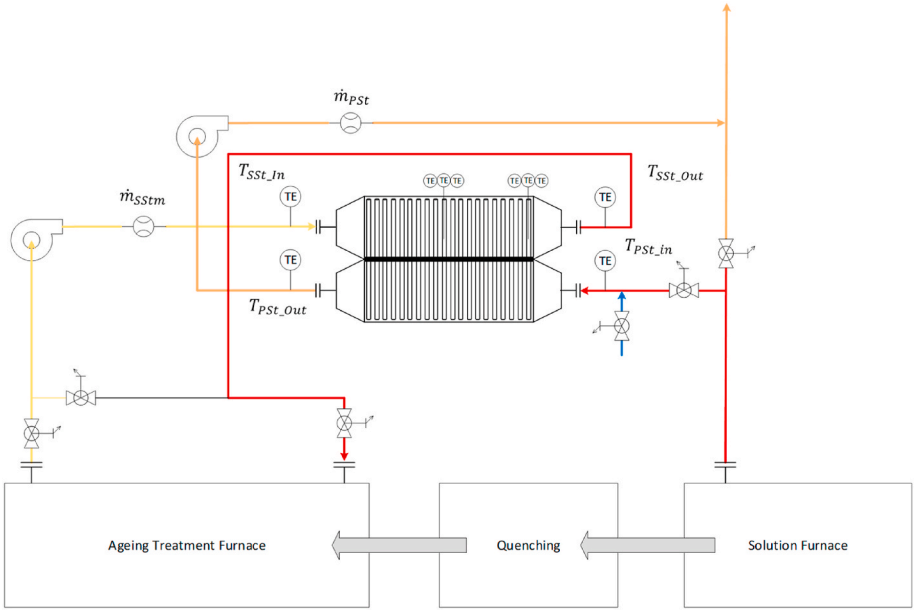

Fig. 13. P&ID of the HPHE installation.

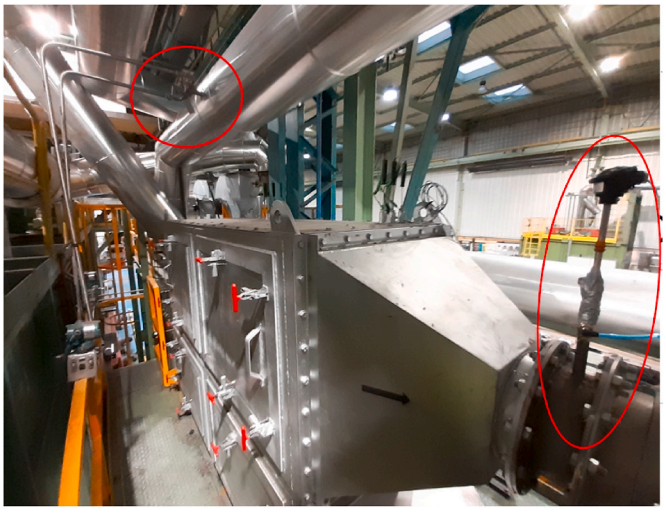

Fig. 14. Photo of the waste heat recovery system where the pitot, to measure the secondary stream velocity, and the thermocouple, to measure the secondary stream outlet temperature, can be seen.

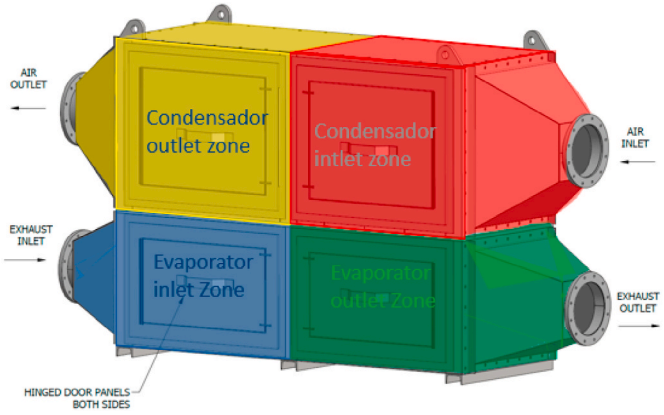

Fig. 15. Four zones of the HPHE external surface.

can be seen in Fig. 14.

3.5. Method of data analysis

3.5.1. HPHE heat loss to the ambient

In order to check that all variables were correctly measured, and that the energy balance is met, thermal losses from the HPHE external surfaces were estimated assuming four different thermal zones: evaporator inlet zone, evaporator outlet zone, condenser inlet zone and condenser outlet zone, as shown in Fig. 15.

The radiative and convective thermal losses from the HPHE external surfaces are estimated following the next equation

$$Q_{losses} = Q_{Rad\_losses} + Q_{Conv\_losses} \tag{24}$$

The radiative thermal losses are calculated for each of the four zones by the equation:

$$Q_{Rad\_losses} = \sum_{i}^{4} \left[A_i \bullet \varepsilon \bullet \sigma \bullet \left(T_i^4 - T_{amb}^4 \right) \right] \tag{25}$$

The convective thermal losses for each of the four zones are calculated by the equation:

$$Q_{Conv\_losses} = \sum_{i}^{4} \left[A_i \bullet h \bullet \left(T_i - T_{amb} \right) \right] \tag{26}$$

where.

A_i is the external surface of each zone (m^2).

σ, Is the Stephan-Boltzmann constant $5.6696x10^{-8}$ W m^{-2} K^{-4}

T_i is the surface temperature of the external surface of each of the four HPHE zones (K).

T_{amb} is the ambient temperature; h is the convective heat transfer coefficient.

3.5.2. Mean efficiency of heat recovery

The instantaneous recovery efficiency in the primary side was calculated based on the following Equation:

$$E = \frac{\dot{m}_{evap} * c_p * (T_{in} - T_{out})}{\dot{m}_{evap} * c_p * (T_{in} - 25)} \quad (27)$$

where the ambient temperature is assumed to be 25 °C.

3.5.3. Total thermal energy recovery

The instantaneous power is multiplied by the time step which comes from the data acquisition frequency and thus the instantaneous thermal energy recovered (MWh) is calculated. The total thermal energy recovered in the monitored period is obtained by summing all the instantaneous values.

3.6. Return on investment calculation

It is a necessity for emerging HPHE technology to have a reasonable return on investment (ROI) in order to be widely adopted. Previous use of this methodology for a similar application has been reported in Ref. [55]. This section deals with a ROI analysis of the installed exhaust to air HPHE unit to determine the potential payback. ROI measures the gain or loss generated on an investment relative to the amount of money invested and is typically seen as a percentage per year or the amount of time taken to break even, shown by Equation (28). This unit was installed as part of a research project so unnecessary R&D costs have been removed to give an indication of a commercial sale.

$$ROI = \frac{Cumulative\ Cash\ Flow}{Annual\ Net\ Benefit\ (ANB)} \quad (28)$$

For this design, costs have been attributed to initial capital and ongoing installation, operational and maintenance costs. Cumulative Cash Flow is considering the total system cost (HPHE and installation cost). Annual Net Benefit (ANB) is the savings attributed to the installation, in this case, reduced energy consumption and reduction in carbon emissions minus operating and maintenance costs and additional operating expenditures like increased electricity, described by Equations (*29-34*):

$$ANB = C_{saved\_NG} + C_{CO2\_emissions\_saved} - E_P - C_{O\&M} \quad (29)$$

where:

$$C_{saved\_NG} = P\dot{Q}_{NG\_saved} \times C_{NG} \times R_{time,HPHE} \quad (30)$$

and

$$C_{CO2\_emissions\_saved} = m_{CO2\_saved} \times C_{CO2\_emission} \quad (31)$$

and

$$E_P = C_{El} \times Q_P \times R_{time,HPHE} \quad (32)$$

and

$$P\dot{Q}_{NG\_saved} = \dot{Q} \times Eff_{PEN} \quad (33)$$

and

$$m_{CO2\_saved} = P\dot{Q}_{NG\_sav} \times F_{NG} \quad (34)$$

Table 1 describes the description, symbols, and units for the ROI calculation. The energy costs used for the ROI calculation have been taken from the quarterly reports on European gas and electricity markets performed by the European Commission for Q1 2022 [56,58], respectively.

The capital cost of the HPHE was €52,151. Installation costs were at a value of €101,726. €600 a year maintenance costs were assumed other than in years 5 and 10, when they were €2368. Annual energy cost increases and annual inflation of 2.5% were assumed. Results of the ROI calculation are shown later in Section 4.2.

Table 1
Description, symbol, value and units used to determine ROI.

Description	Symbol	Value	Unit
Reduction in natural gas saving	Cs_{aved_NG}	$PQ_{NG,saved} \times C_{NG} \times R_{time,\ HPHE}$	€.yr^{-1}
Total CO2 cost saving	$C_{CO2\_emission\_saved}$	$m_{CO2\_saved} \times C_{CO2\_emission}$	€.yr^{-1}
Parasitic load energy cost	E_P	$C_{El} \times Q_P \times R_{time,\ HPHE}$	€.yr^{-1}
Cost of maintenance	$C_{O\&M}$		€.yr^{-1}
Primary energy savings	$PQ_{NG,sav}$	$*QEff_{pen}$	MWh
Natural gas cost	C_{NG}	97 [56]	€.MWh-1
Working hours of the system per year	$R_{time,\ HPHE}$	5100	hr.y-1
Mass of CO2 emissions prevented	m_{CO2_saved}	$PQ_{NG,saved}$ x F_{NG}	t_{CO2eq}. y^{-1}
CO_2 emission cost	$C_{CO2\_emission}$	89.52 [57]	€.tCO2e-1
Electrical energy cost	C_{El}	201 [58]	€.MWh-1
Additional electricity load	Q_P		kW
Thermal power recovered by the HPHE		$\dot{m} \times C_p \times (T_{h,in} - T_{h,out})$	J.s-1 (W)
Conversion factor to determine weight of natural gas saved per MWh	F_{NG}	181	kg_{CO2}. MWh^{-1}
Well-to-tank emissions factor	Eff_{Pen}	1.01	–

4. Results and discussion

4.1. Performance of the waste heat recovery solution

In the following, the performance of the waste heat recovery solution is shown for the 6 months in which data have been collected up to now with a total operating time of the system of 1893 h. That is, except for occasional stops, the facilities (the solution furnace, the ageing furnaces and the ETEKINA HPHE heat recovery system) have been in continuous operation from Monday to Friday and, in some cases, until Saturday noon. The furnaces carried out a planned shutdown at Christmas to carry out maintenance operations and it has also stopped for a few days for production reasons.

In the period monitored (1893 h), the system has registered a thermal energy recovery of 166 MWh on the primary side; instantaneous measurements of the waste heat stream inlet and outlet temperature (Fig. 16) and of the flow rate (Fig. 17) are used to calculate the instantaneous power (kW) recovered from the waste heat stream (Fig. 18) (see Fig. 19).

The mean efficiency of the heat recovery has been 48% in the monitored period.

Table 2 provides a comparison between the data used for the design of the HPHE and the averaged data monitored during 6 months. The actual flow rate of the exhaust has been slightly lower than the design value. In the case of the secondary stream, the actual flow rate is close to the design value.

The primary stream temperature at the inlet of the HPHE evaporator was the same as expected during the design of the HPHE. The primary stream temperature at the outlet of the HPHE evaporator was 8% lower than expected during the design of the HPHE and the primary flow rate was also 10% lower. Transferred power at the primary stream results are as expected. The measured temperature of the secondary stream at the inlet of the condenser was much higher than the design value; this adversely affected the HPHE performance since there was a lower temperature difference between the primary and secondary streams.

The total unit duty was designed for a heat recovery rate of 89 kW, but operates at approximately 61 kW. The difference observed is mainly due to leaks through the diverter valve and due to thermal losses from the HPHE external surface. The leaks in the diverter valve mean that part of the secondary stream returns back to the HPHE inlet, bypassing the solution furnace. Therefore, less energy goes into the solution furnace

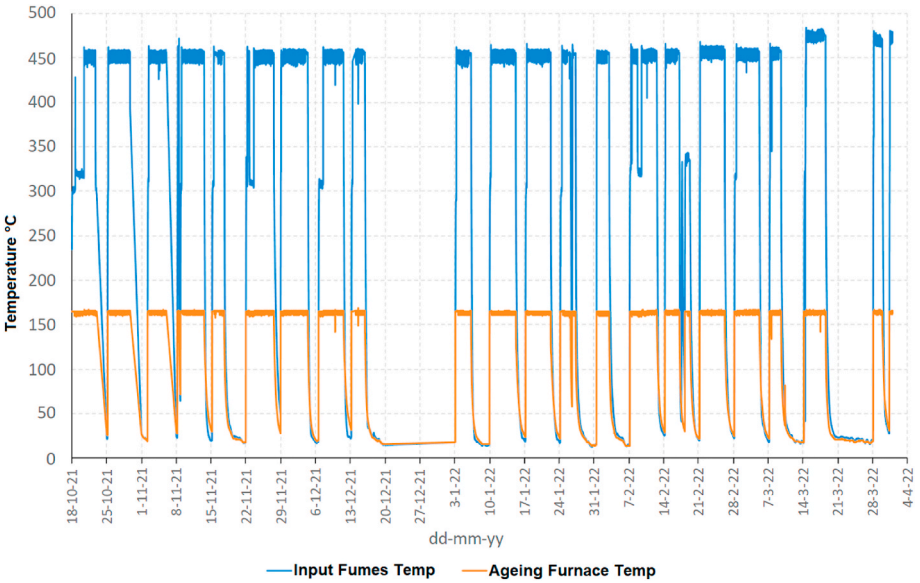

Fig. 16. Instantaneous measurements of the waste heat stream inlet and outlet temperature during the monitored period.

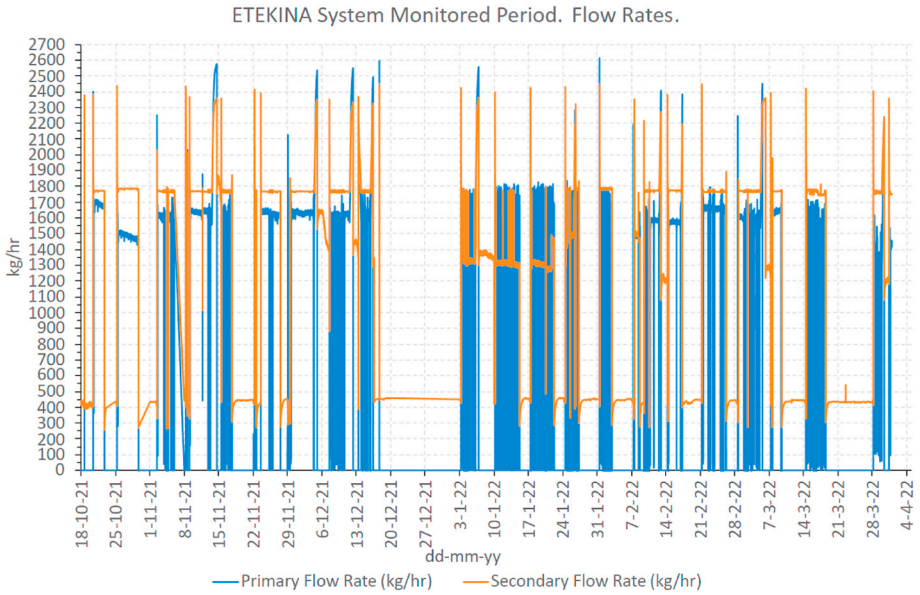

Fig. 17. Primary and secondary flow rates measured during the monitored period.

and, at the same time, the HPHE air entry temperature increases. Therefore, the heat transfer in the HPHE is diminished due to a lower temperature difference between the hot and cold streams.

Deviations in the stream flow rates were observed as being due to problems identified with a diverter valve and a valve installed at the outlet of the ageing furnace. Failures in the diverter valve activated the bypass valve and, consequently, the primary stream flow rate fluctuated during certain periods. On the other hand, problems with the valve installed at the outlet of the ageing furnace reduced the secondary stream flow rate. Leaks in the valves seem to be the major reason for these problems, as the valves installed seem not to be totally reliable after having run a long period at high temperature.

Additionally, it was observed that some parts of the waste heat recovery system were initially uninsulated (solution furnace outlet, HPHE, diverter valve and 2-way valve) and this was only rectified at the very end of the monitored period, causing an increase in the inlet temperature to the waste heat recovery system (blue line in Fig. 16).

Despite these factors, the impact of the waste heat recovery solution on the natural gas consumption of the ageing furnace is clearly seen in Fig. 20, which shows the daily natural gas consumption of the ageing furnace. The variation between the different green points comes from the variation in production. The number of parts that are treated each day are not consistent, for example, they have differing geometry and weight. Therefore, the energy required for the thermal treatment is not the same either. However, two different levels of natural gas consumption can be identified in the Figure. During the two periods with a lower natural gas consumption, the HPHE was working correctly. In the period with a higher natural gas consumption, one of the valves of the waste heat recovery installation broke down and thus there was no waste heat recovery. The Figure clearly shows that almost 50% of the ageing furnace gas consumption is saved when the waste heat recovery system is working.

Table 3 summarises the most significative results obtained during the monitored period from an energetic point of view. The monitored period

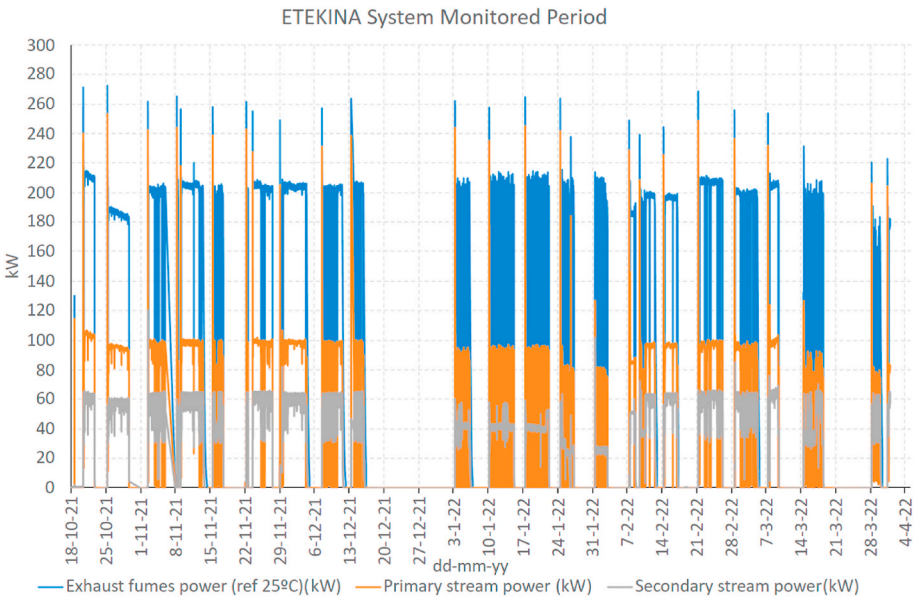

Fig. 18. Instantaneous thermal power recovered in the waste heat stream (blue) calculated based on data from Figs. 16 and 17.

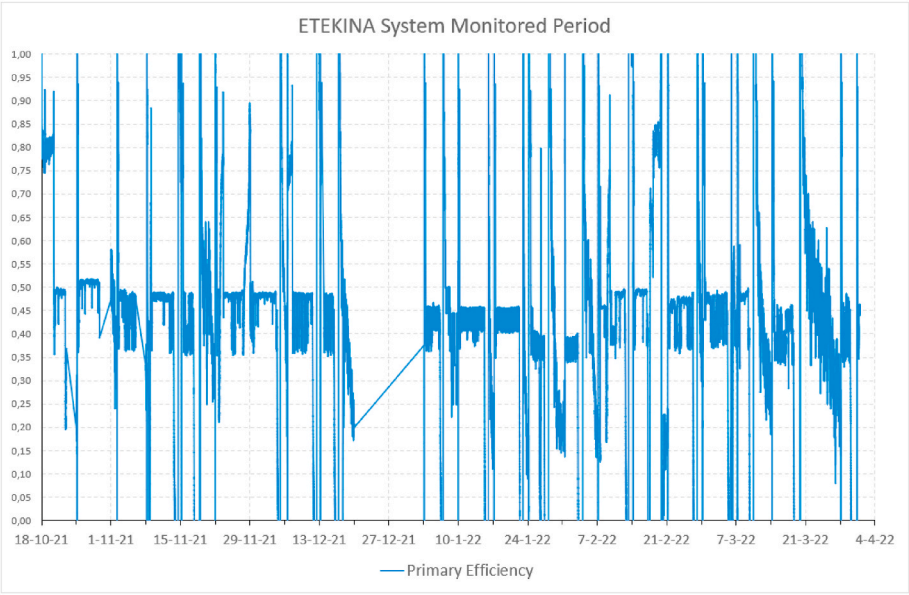

Fig. 19. Instantaneous efficiency in the primary side.

Table 2
Comparison between design data and monitored data.

	Design Data	Real Data
Mass flow rates		
Exhaust, kg·hr^{-1}	1791	1623
Air, kg·hr^{-1}	1802	1762
Temperatures		
Exhaust entry, °C	400	400
Exhaust exit, °C	240	220
Air entry, °C	145	199
Air exit, °C	317	303
Heat recovered		
Total unit duty, kW	88.6	61

the system worked was 1893 h. However, for the energy analysis, 885 h have been considered as representative of a good system performance, this being days when issues with the valves did not occur. Annual estimations carried out, extrapolating the energy performance results obtained during those 885 h to the 5100 working hours that could be expected per year, are also included in Table 3. Finally, Table 3 also includes the results that could be expected when best engineering practices are applied, such an insulation of the HPHE and the ducting, optimised valve sizing, higher tightness check of the exhaust and hot gas line. 476 MWh of natural gas savings could be expected per year and a reduction of CO_2 emissions of 86 tonnes per year.

From the results obtained during the applicable monitored period, it can be observed that the thermal power recovered by the primary stream was 97 kW, while the thermal power transferred to the secondary stream was 61 kW. Based on the external surface areas of each zone (evaporator inlet and outlet zone external surfaces of 3.64 m^2 and condenser inlet

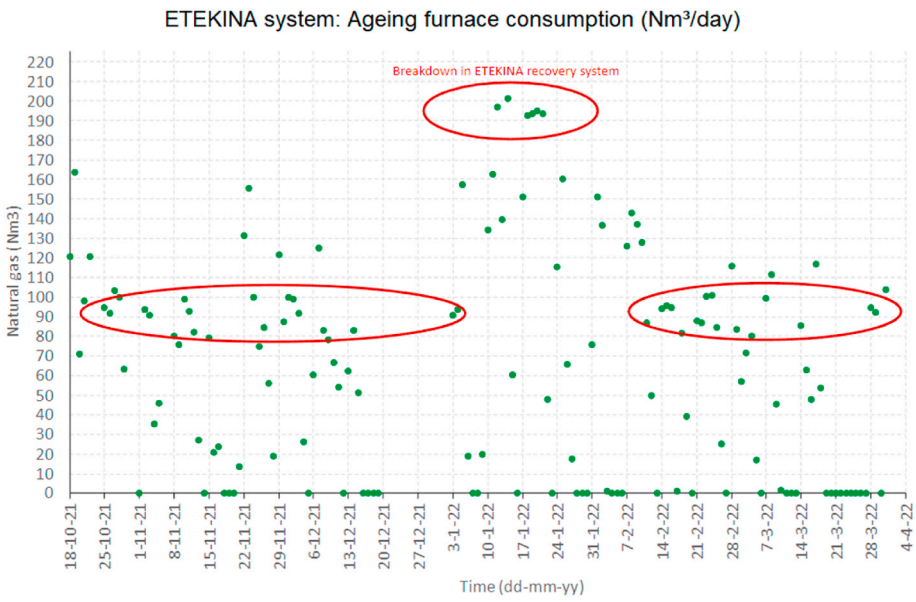

Fig. 20. Ageing furnace gas consumption (Nm3. day^{-1}).

Table 3
Main results of the waste heat recovery system from an energetic point of view.

	Data extrapolated from real measurements	Expected results for Best Engineering Practices
Exhaust fumes power referred to 25 °C, MW	0.203[a]	0.203
Available energy in the exhaust, MWh	180[b] (885 h)	1035 (per year)
HPHE primary efficiency, %	48	48
Thermal energy recovered by primary stream, MWh	86 (885 h)	496 (per year)
HPHE secondary efficiency, %	63	96[f]
Thermal energy transferred to secondary stream, MWh	54[c] (885 h)	476 (per year)
Facility efficiency, %	62	90[g]
Thermal energy transferred to furnace, MWh	34	
Operating hours during monitored period, h	885	
Expected annual working hours, h.year^{-1}	5100	5100
Annual thermal energy transferred to furnace, MWh.year^{-1}	196	428
Annual primary energy savings from Natural Gas, MWh.year^{-1}	218[d]	476[d]
Annual CO_2 emission reduction, $TnCO_2$.year^{-1}	39,5[e]	86[e]
Annual electricity consumption, MWh.year^{-1}	50.85	33.66[h]

[a] Average power (blue line in Fig. 18).
[b] Average power (blue line in Fig. 18) X 885 h.
[c] Average power (grey line in Fig. 18) X 885 h.
[d] Conversion factor (natural gas to primary energy. LHH = 0.9 *HHV).
[e] Conversion factor to determine weight of natural gas saved per MWh, 181 kg_{CO2}. MWh^{-1}.
[f] By improving the system insulation and improving the diverter valve performance.
[g] By improving the system insulation and by optimizing the control strategy.
[h] By optimizing the fans size and by adding speed controllers.

and outlet zone external surfaces of 4.085 m^2) and using local temperature measurements made on each zone representative of four surface points (evaporator inlet zone temperature, 248 °C; evaporator outlet zone temperature, 148 °C; condenser inlet zone temperature, 138 °C and condenser outlet temperature, 132 °C), assuming a conservative value of emissivity of 0.7 as the HPHE is covered by a metallic paint and considering a value of 7 W m^{-2} K^{-1} as convective heat transfer coefficient, the thermal losses from the HPHE external surface were estimated using Equations (25) and (26). The estimated thermal losses reach a value in the region of 35 kW, which is approximately the difference between the thermal power recovered by the primary stream (97 kW) and the thermal power transferred to the secondary stream (61 kW).

4.2. Economic analysis

The economic analysis and the calculation of the ROI are based on the performance expected from the HPHE once best engineering practices are applied (3rd column in Table 3). 93 kW could be expected to be transferred to the ageing furnace, resulting in 476 MWh.year^{-1} of natural gas savings. In consequence, an annual reduction of 86 tons of CO_2 could also be expected. In addition, an annual electricity consumption of 33.6 MWh.year^{-1} could be expected due to the fans installed in the waste heat recovery system. Considering a gas price of 97 €/MWh [56], a CO2 emission cost of 89.52 €.Tn^{-1} [57], an electricity price of 201 €/MWh [58] and the unit, installation and maintenance costs mentioned in Section 4.1, the expected ROI of the waste heat recovery system is 35 months. A spread of the cash flow can be seen in Fig. 21.

Further details on the calculation can be found in Table 4.

4.3. HPHE performance during steady state process operation

The data were collected for a duration of around 18 h of a steady state operation of the processes. The experimental measurements of mass flow rates of exhaust and air are presented in Fig. 22. The exhaust mass flow rate was around 1676 kg h^{-1}, while the air mass flow rate was approximately 1772 kg h^{-1}. The inlet and outlet temperatures of the exhaust flue gas and the air stream measurements are shown in Fig. 23.

It can be observed that the air outlet temperature variation was synchronised with variations of the air inlet temperature but with smoother peaks. The exhaust inlet temperature was 400 °C while the outlet temperature was 215.9 °C. The air inlet temperature was 194.7 °C, and the outlet temperature was 342.6 °C. It can be noticed that the air outlet temperature was higher than the exhaust outlet temperature as a result of the counter-current design of the HPHE considering

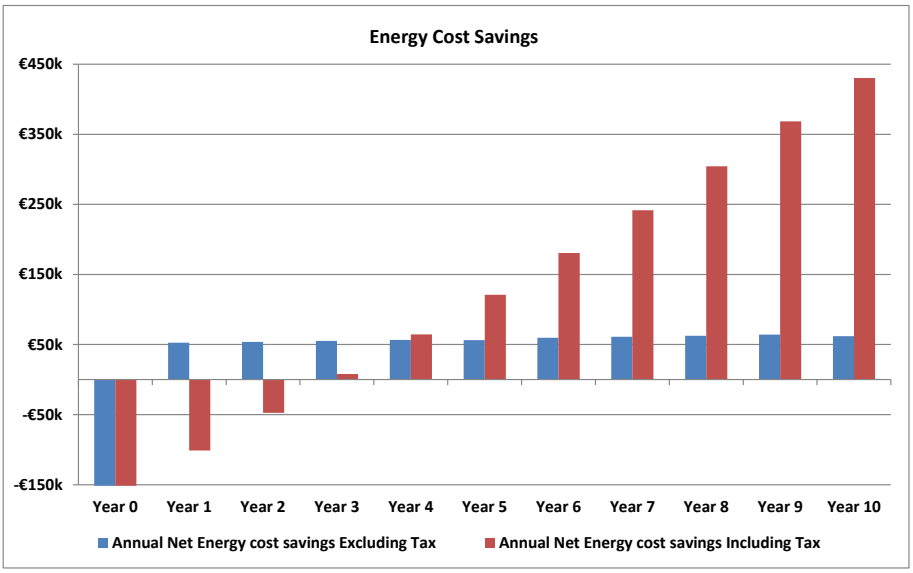

Fig. 21. Cash flow of installation.

Table 4
Expected results for Best Engineering Practices.

	Expected results for Best Engineering Practices
Annual primary energy savings from Natural Gas, MWh.year^{-1}	476
Annual gas natural savings, €.year^{-1}	44,555
Annual CO2 emission reduction, TnCO2. year^{-1}	86
Annual savings in the CO2 emission cost, €. year^{-1}	7698
Annual electricity consumption, MWh.year^{-1}	33.66
Annual electricity cost, €/.year^{-1}	5680
HPHE unit cost, €	52,151
Installation cost, €	101,726
Maintenance cost, €.year^{-1}	600
ROI, years	35 Months

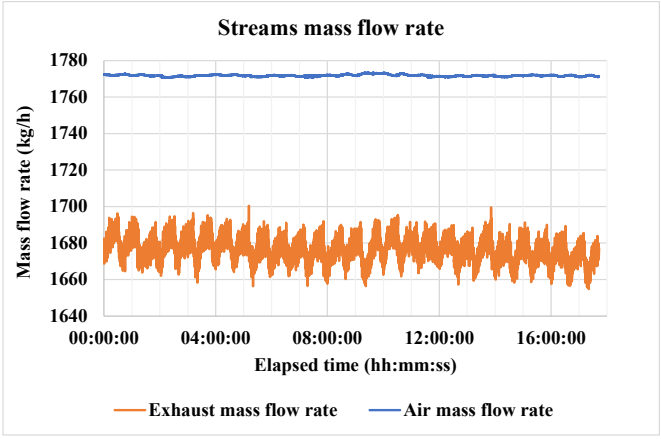

Fig. 22. Experimental mass flow rates of exhaust and air streams.

that the air and the exhaust had similar flow rates and specific heat capacity.

The heat transfer rate from the exhaust and heat transfer rate to the air are presented in Fig. 24. It can be observed that the heat transfer rate from the exhaust was around 95 kW while only 54 kW was absorbed by the air stream. A HPHE is a system that transfers all the heat absorbed when it is functioning properly. Hence, the difference in heat between the two streams was transferred to the ambient as heat losses by radiation and natural convection. This clearly highlights the importance of insulation to minimise the heat losses and maximise efficiency.

4.4. Theoretical modelling results

In order to predict the thermal performance of the HPHE, the average experimental values of 18 h measurements were input into the theoretical model. These included the inlet temperatures and flow rates into the HPHE of both the flue gas exhaust and the air. The thermal performance prediction of the HPHE includes the outlet temperatures of the exhaust and air streams in addition to the heat recovery rate and thermal effectiveness. The experimental and theoretical predictions of the outlet temperatures of the flue gas and air are illustrated in Fig. 25. The theoretical model predicted an outlet temperature of the exhaust at 246.2 °C while the average experimental outlet temperature was 216.1 °C. Furthermore, the predicted air outlet temperature was 350.5 °C while the experimental one was 300.4 °C. Furthermore, both exhaust and air had similar temperature trends since the heat capacity rate was similar, while both streams had outlet temperatures lower than the predictions. This indicated that the deviation between the predictions and the experimental values was due to the heat losses from the HPHE by radiation and natural convection in addition to the accuracy of the correlations used in the model.

The predicted heat recovery rate by the model was 79.7 kW while the total heat transferred from the exhaust was 95.3 kW and the overall heat gained by the air stream was 53.7 kW as shown in Fig. 24. It can be noticed that deviation between the theoretical model and the heat transfer from the exhaust is around 20% since the prediction tool does not account for heat losses and assumes the HPHE with the streams is an adiabatic system. In addition, the modelling tool assumes that the flow rates are constant and neglects the fluctuations on stream inlet temperatures. The effectiveness of the HPHE based on the heat recovery predicted was 79.4% while it was around 56.5% based on the heat recovered by the air. The modelling tool prediction accuracy can be further improved by accounting for heat loss calculations. However, it is vital to insulate the external case to enhance the HPHE recovery to the maximum possible value and improve the overall system efficiency.

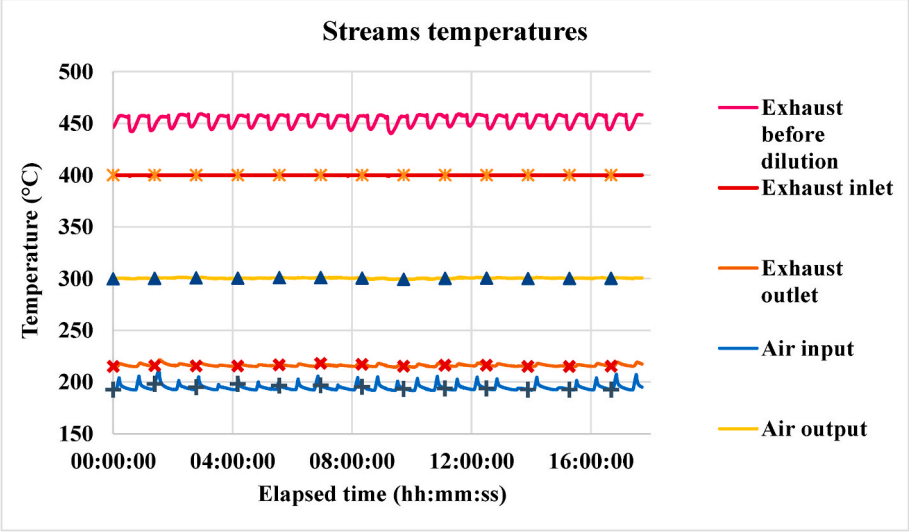

Fig. 23. HPHE streams temperatures.

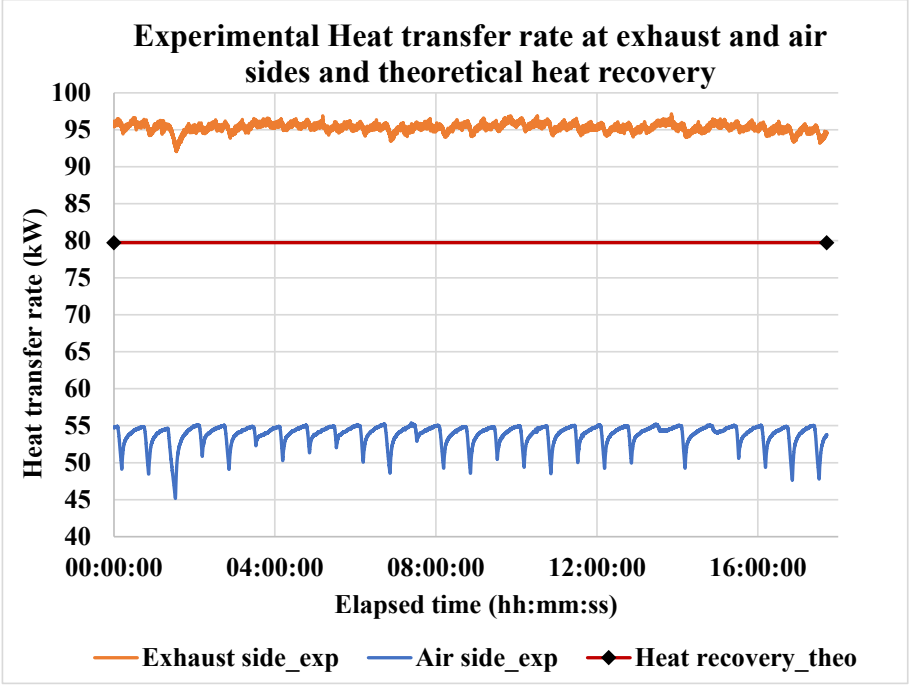

Fig. 24. Heat transfer rate from exhaust stream and to the air stream.

5. Conclusion

A HPHE was installed to recover heat from a solution heat treatment furnace used within the aluminium industry and was investigated experimentally and theoretically. The HPHE installed in the plant recovered 97 kW from the exhaust stream of the furnace, from which 61 kW was transferred to the secondary stream.

The study highlights the development of a novel and industry ready technology as the installed HPHE currently has a ROI of 35 months, which highlights the success of heat pipe technology within the aluminium industry. In the case presented, the expected primary energy reduction at the ageing furnace could be expected to be 476 MWh. $year^{-1}$ with an estimated CO_2 emissions reduction of 86 tCO_2. $year^{-1}$ when best engineering practices are applied.

The theoretical model which was developed to predict the thermal performance of the HPHE showed a heat recovery of 79.7 kW with a 20% deviation from the experimental results. The development of the theoretical model provides an analysis for evaluating the HPHE technology and accessing the replicability potential. The model can be adjusted for a variety of operational conditions, temperatures, and the design of a HPHE unit. This can allow the rapid expansion of HPHEs within the aluminium industry, which can further lower greenhouse gas emissions. The accuracy of the HPHE model could be improved by implementing the heat loss calculations within the prediction. Using the current validated modelling tool, the system could also be applied to various industrial sites where the implementation of waste heat recovery techniques is needed. Other consideration in the presented work will need to be further investigated such as fouling handling or condensation of exhaust gases. Indeed, the presented scope aimed to achieve waste heat recovery from an exhaust with low particulate and low water

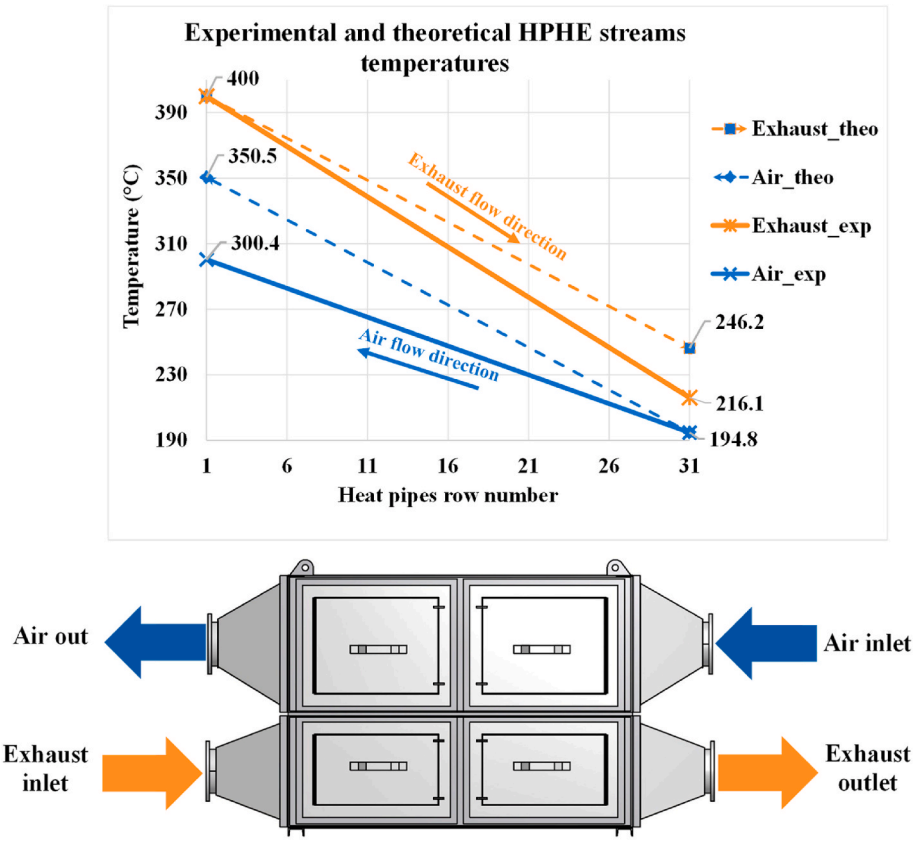

Fig. 25. Comparison between the experimental and theoretical temperature predictions using the modelling tool.

content. However, some industrial cases will require condensation of the exhaust, recovering the latent heat of evaporation, causing acid and water to condense on the heat pipes. The same can be said about fouling. There is currently very limited research done through this approach to waste heat recovery.

It is also important to highlight that the ETEKINA project has allowed the novel application of HPHE technology in process industries where traditional heat exchangers have failed. The success of the ETEKINA project is expected to be a reference for future applications of this technology.

Author statement

All persons who meet authorship criteria are listed as authors, and all authors certify that they have participated sufficiently in the work to take public responsibility for the content, including participation in the concept, design, analysis, writing, or revision of the manuscript. Furthermore, each author certifies that this material or similar material has not been and will not be submitted to or published in any other publication before its appearance in Energy. Please indicate the specific contributions made by each author (list the authors' initials followed by their surnames, e.g., Y.L. Cheung). The name of each author must appear at least once in each of the three categories below. Conception and design of study: All Authors. Drafting the manuscript: All Authors. Approval of the version of the manuscript to be published (the names of all authors must be listed):

Declaration of competing interest

The authors declare that they have no known competing financial interests or personal relationships that could have appeared to influence the work reported in this paper.

Data availability

Data will be made available on request.

Acknowledgements

The authors would like to thank the European Commission and the partners of the European H2020 project "Heat pipe technology for thermal energy recovery in industrial applications" (https://www.etekina.eu/, H2020-EE-2017-PPP- 768772) for their support.

Additional information is available in the project Web page www.etekina.eu or www.etekina.com.

All persons who have made substantial contributions to the work reported in the manuscript (e.g., technical help, writing and editing assistance, general support), but who do not meet the criteria for authorship, are named in the Acknowledgements and have given us their written permission to be named. If we have not included an Acknowledgements, then that indicates that we have not received substantial contributions from non-authors.

References

[1] About - Etekina n.d. https://www.etekina.eu/about/(accessed March 26, 2022).
[2] Jouhara H, Montorsi L, Sayegh MA. Advances and applications of renewable energy. Renew Energy 2021;165:75–6. https://doi.org/10.1016/J.RENENE.2020.11.092.
[3] World Bank Open. Data | Data n.d, https://data.worldbank.org/. [Accessed 27 November 2021]. accessed.
[4] CO2 emissions – global energy review. Analysis - IEA n.d 2021. https://www.iea.org/reports/global-energy-review-2021/co2-emissions. [Accessed 27 November 2021]. accessed.

[5] EUR-Lex - 52011DC0112 - EN - EUR-Lex n.d. https://eur-lex.europa.eu/legal-content/EN/ALL/?uri=CELEX:52011DC0112 (accessed November 28, 2021).
[6] Olabi AG, Abdelkareem MA. Energy storage systems towards 2050. Energy 2021; 219:119634. https://doi.org/10.1016/J.ENERGY.2020.119634.
[7] Guzović Z, Duić N, Piacentino A, Markovska N, Mathiesen BV, Lund H. Paving the way for the paris agreement: contributions of SDEWES science. Energy 2022: 125617. https://doi.org/10.1016/J.ENERGY.2022.125617.
[8] Jouhara H. Waste heat recovery in process industries. Weinheim: Wiley; 2022.
[9] Miró L, Brückner S, Cabeza LF. Mapping and discussing Industrial Waste Heat (IWH) potentials for different countries. Renew Sustain Energy Rev 2015;51: 847–55. https://doi.org/10.1016/J.RSER.2015.06.035.
[10] Energy prices and costs in Europe. Communication from the commission to the European parliament, the council, and the European economic and social committee and the committee of the regions n.d. https://eur-lex.europa.eu/legal-content/EN/ALL/?uri=CELEX:52014DC0021 (accessed March 26, 2022).
[11] Commission E, Energy D-G for, Heald S, Debrosses N, Rademaekers K, Moerenhout J, et al. Study on energy prices, costs and subsidies and their impact on industry and households : final report. Publications Office; 2019. https://doi.org/10.2833/825966.
[12] Brueckner S, Miró L, Cabeza LF, Pehnt M, Laevemann E. Methods to estimate the industrial waste heat potential of regions – a categorization and literature review. Renew Sustain Energy Rev 2014;38:164–71. https://doi.org/10.1016/J.RSER.2014.04.078.
[13] Luo S, Hu W, Liu W, Xu X, Huang Q, Chen Z, et al. Transition pathways towards a deep decarbonization energy system—a case study in Sichuan, China. Appl Energy 2021;302:117507. https://doi.org/10.1016/J.APENERGY.2021.117507.
[14] Haraldsson J. Improved energy efficiency in the aluminium industry and its supply chains. Linköping Studies in Science and Technology Dissertation 2020:2063.
[15] Thekdi AC. Industrial waste heat recovery: potential applications. 2014. Available Technologies and Crosscutting R&D Opportunities.
[16] Waste heat recovery methods and technologies - Chem Eng | Page 2 n.d. https://www.chemengonline.com/waste-heat-recovery-methods-and-technologies/?pagenum=2 (accessed March 27, 2022).
[17] Brough D, Jouhara H. The aluminium industry: a review on state-of-the-art technologies, environmental impacts and possibilities for waste heat recovery. International Journal of Thermofluids 2020;1–2:100007. https://doi.org/10.1016/J.IJFT.2019.100007.
[18] Guzović Z, Duic N, Piacentino A, Markovska N, Mathiesen BV, Lund H. Recent advances in methods, policies and technologies at sustainable energy systems development. Energy 2022;245:123276. https://doi.org/10.1016/J.ENERGY.2022.123276.
[19] Electricity prices around the world | GlobalPetrolPrices.com n.d. https://www.globalpetrolprices.com/electricity_prices/(accessed March 26, 2022).
[20] Natural gas prices around the world. GlobalPetrolPrices.com n.d. https://www.globalpetrolprices.com/natural_gas_prices/; June 2021 (accessed March 26, 2022)
[21] Yanjia W, Chandler W. The Chinese nonferrous metals industry—energy use and CO2 emissions. Energy Pol 2010;38:6475–84. https://doi.org/10.1016/J.ENPOL.2009.03.054.
[22] Aluminium – Analysis - IEA. accessed March 26, 2022), https://www.iea.org/reports/aluminium.
[23] Jouhara H, Sayegh MA. Energy efficient thermal systems and processes. Therm Sci Eng Prog 2018;7:e1–2. https://doi.org/10.1016/J.TSEP.2018.07.016.
[24] Ros-Dosdá T, Fullana-i-Palmer P, Mezquita A, Masoni P, Monfort E. How can the European ceramic tile industry meet the EU's low-carbon targets? A life cycle perspective. J Clean Prod 2018;199:554–64. https://doi.org/10.1016/J.JCLEPRO.2018.07.176.
[25] Enderle P, Nowak O, Kvas J. Potential alternative for water and energy savings in the automotive industry: case study for an Austrian automotive supplier. J Clean Prod 2012;34:146–52. https://doi.org/10.1016/J.JCLEPRO.2011.11.013.
[26] Bonilla-Campos I, Nieto N, del Portillo-Valdes L, Egilegor B, Manzanedo J, Gaztañaga H. Energy efficiency assessment: process modelling and waste heat recovery analysis. Energy Convers Manag 2019;196:1180–92. https://doi.org/10.1016/J.ENCONMAN.2019.06.074.
[27] Cui J, Roven HJ. Recycling of automotive aluminum. Trans Nonferrous Metals Soc China 2010;20:2057–63. https://doi.org/10.1016/S1003-6326(09)60417-9.
[28] Study on energy efficiency and energy saving potential in industry and on possible policy mechanisms. https://energy.ec.europa.eu/study-energy-efficiency-and-energy-saving-potential-industry-and-possible-policy-mechanisms_en (accessed March 26, 2022).
[29] Jouhara H, Olabi AG. Editorial: industrial waste heat recovery. Energy 2018;160: 1–2. https://doi.org/10.1016/J.ENERGY.2018.07.013.
[30] Egilegor B, Jouhara H, Zuazua J, Al-Mansour F, Plesnik K, Montorsi L, et al. ETEKINA: analysis of the potential for waste heat recovery in three sectors: aluminium low pressure die casting, steel sector and ceramic tiles manufacturing sector. International Journal of Thermofluids 2020;1–2:100002. https://doi.org/10.1016/J.IJFT.2019.100002.
[31] Gu X, Chen W, Chen C, Li N, Gao W, Wang Y. Detailed characteristics of fluid flow and its effect on heat transfer in shell sides of typical shell-and-tube heat exchangers. Int J Therm Sci 2021:107381. https://doi.org/10.1016/J.IJTHERMALSCI.2021.107381.
[32] Panday NK, Singh SN. Thermo-hydraulic performance analysis of multi-pass chevron type plate heat exchanger. Therm Sci Eng Prog 2020;16:100478. https://doi.org/10.1016/J.TSEP.2020.100478.
[33] He L, Li P. Numerical investigation on double tube-pass shell-and-tube heat exchangers with different baffle configurations. Appl Therm Eng 2018;143:561–9. https://doi.org/10.1016/J.APPLTHERMALENG.2018.07.098.
[34] Jouhara H, Almahmoud S, Brough D, Guichet V, Delpech B, Chauhan A, et al. Experimental and theoretical investigation of the performance of an air to water multi-pass heat pipe-based heat exchanger. Energy 2021;219:119624. https://doi.org/10.1016/J.ENERGY.2020.119624.
[35] Robinson AJ, Colenbrander J, Deaville T, Durfee J, Kempers R. A wicked heat pipe fabricated using metal additive manufacturing. International Journal of Thermofluids 2021;12:100117. https://doi.org/10.1016/J.IJFT.2021.100117.
[36] Jouhara H, Fadhl B, Wrobel LC. Three-dimensional CFD simulation of geyser boiling in a two-phase closed thermosyphon. Int J Hydrogen Energy 2016;41: 16463–76. https://doi.org/10.1016/J.IJHYDENE.2016.02.038.
[37] Alizadehdakhel A, Rahimi M, Alsairafi AA. CFD modeling of flow and heat transfer in a thermosyphon. Int Commun Heat Mass Tran 2010;37:312–8. https://doi.org/10.1016/J.ICHEATMASSTRANSFER.2009.09.002.
[38] Pishvar M, Saffar Avval M, Mansoori Z, Amirkhosravi M. Three dimensional heat transfer modeling of gas-solid flow in a pipe under various inclination angles. Powder Technol 2014;262:223–32. https://doi.org/10.1016/J.POWTEC.2014.04.075.
[39] Manimaran R, Palaniradja K, Alagumurthi N, Velmurugan K. An investigation of thermal performance of heat pipe using di-water. Sci Technol 2012;2:77–80. https://doi.org/10.5923/J.SCIT.20120204.04.
[40] Alammar AA, Al-Dadah RK, Mahmoud SM. Numerical investigation of effect of fill ratio and inclination angle on a thermosiphon heat pipe thermal performance. Appl Therm Eng 2016;108:1055–65. https://doi.org/10.1016/J.APPLTHERMALENG.2016.07.163.
[41] Jouhara H, Almahmoud S, Brough D, Guichet V, Delpech B, Chauhan A, et al. Experimental and theoretical investigation of the performance of an air to water multi-pass heat pipe-based heat exchanger. Energy 2021;219:119624. https://doi.org/10.1016/J.ENERGY.2020.119624.
[42] Rohsenow Editor WM, Hartnett Editor JR, Cho Editor YI, San NY, Washington F, Auckland DC, et al. Handbook of heat transfer. 1998.
[43] Rohsenow WM. A method of correlating heat transfer data for surface boiling of liquids. Cambridge, Mass: MIT Division of Industrial Cooporation; 1951. p. 1951.
[44] Guichet V, Almahmoud S, Jouhara H. Nucleate pool boiling heat transfer in wickless heat pipes (two-phase closed thermosyphons): a critical review of correlations. Therm Sci Eng Prog 2019;13. https://doi.org/10.1016/j.tsep.2019.100384.
[45] Nusselt W. The condensation of steam on cooled surfaces. Z Ver Dtsch Ing 1916;60: 541–6.
[46] Guichet V, Jouhara H. Condensation, evaporation and boiling of falling films in wickless heat pipes (two-phase closed thermosyphons): a critical review of correlations. International Journal of Thermofluids 2020;1(2):100001. https://doi.org/10.1016/j.ijft.2019.100001.
[47] Stasiulevicius J, Skrinska A. Heat transfer in banks of finned tubes in crossflow. Vilnius, USSR: Mintis 1974;243:1066–71.
[48] Yudin VF. Teploobmen poperechno orebrennykh trub. Leningrad: Mashinostroenie; 1982.
[49] Kakac S, Shah RK, Aung W. Handbook of single-phase convective heat transfer. United States: John Wiley and Sons Inc; 1987.
[50] Cao E. Heat transfer in process engineering. New York: McGraw-Hill; 2010.
[51] Danielewicz J, Sayegh MA, Śniechowska B, Szulgowska-Zgrzywa M, Jouhara H. Experimental and analytical performance investigation of air to air two phase closed thermosyphon based heat exchangers. Energy 2014;77:82–7. https://doi.org/10.1016/j.energy.2014.04.107.
[52] Holman J. Heat transfer. McGraw-Hill Education; 2009.
[53] Shabgard H, Allen MJ, Sharifi N, Benn SP, Faghri A, Bergman TL. Heat pipe heat exchangers and heat sinks: opportunities, challenges, applications, analysis, and state of the art. Int J Heat Mass Tran 2015;89:138–58. https://doi.org/10.1016/J.IJHEATMASSTRANSFER.2015.05.020.
[54] Bergman TL, Incropera FP, DeWitt DP, Lavine AS. Fundamentals of heat and mass transfer. seventh ed. USA: John Wiley & Sons; 2011.
[55] Brough D, Mezquita A, Ferrer S, Segarra C, Chauhan A, Almahmoud S, et al. An experimental study and computational validation of waste heat recovery from a lab scale ceramic kiln using a vertical multi-pass heat pipe heat exchanger. Energy 2020;208. https://doi.org/10.1016/j.energy.2020.118325.
[56] European commission. Quarterly report on European gas markets market observatory for energy DG energy. 2022.
[57] Ember. EU Carbon Price Tracker 2022. https://Ember-ClimateOrg/Data/Data-Tools/Carbon-Price-Viewer/.
[58] European commission. Quarterly report on European electricity markets market observatory for energy DG energy. 2022.